Formation of disorder aluminium zones in an immiscible lead–aluminium system

2004 J. Phys.: Condens. Matter 16 1131

(http://iopscience.iop.org/0953-8984/16/7/013)

INSTITUTE OF PHYSICS PUBLISHING JOURNAL OF PHYSICS: CONDENSED MATTER

J. Phys.: Condens. Matter **16** (2004) 1131–1140 PII: S0953-8984(04)72167-0

Formation of disorder aluminium zones in an immiscible lead–aluminium system

R Z Huang, L H Zhang, M L Sui and Y M Wang[1]

Shenyang National Laboratory for Materials Science, Institute of Metal Research, Chinese Academy of Sciences, Shenyang 110016, People's Republic of China

E-mail: ymwang@imr.ac.cn

Received 17 November 2003
Published 6 February 2004
Online at stacks.iop.org/JPhysCM/16/1131 (DOI: 10.1088/0953-8984/16/7/013)

Abstract

High resolution transmission electron microscopy (HRTEM) observations show evidence for the formation of disorder Al zones around some faceted Pb inclusions embedded in an Al matrix in immiscible lead–aluminium samples, which were prepared by a melt-spun method and then aged for about two months at room temperature. Furthermore, it is found that, both before and after ageing, all such Pb inclusions have a cube–cube orientation relationship with the Al matrix. The results of molecular dynamics (MD) simulations give an extensive analysis of the formation of the disorder Al zones and provide a reasonable explanation for the HRTEM finding: the existence of oxygen soluted in the Pb inclusions at higher temperatures may lead to the formation of the disorder Al zone in the aged sample. The dependence of the thickness of the disorder Al zone on the amount of oxygen soluted in the Pb inclusion at higher temperatures, and the average stress in the equilibrium configuration of a MD cell, is discussed.

1. Introduction

A number of studies have been performed on microstructural, dynamical and thermal properties in miscibility gap alloys, and in particular in binary alloys with positive enthalpy of mixing ($+\Delta H$) [1–4]. The structural characteristics of amorphous alloys formed in such immiscible systems [5–8] are different from those of glasses formed in $-\Delta H$ systems. In the latter systems, chemical short-range ordering develops as a thermodynamic driving force to drive the constituent elements to intermix to maximize the number of unlike bonds. In contrast to systems with a negative heat of mixing, amorphous alloys formed in systems with a positive enthalpy of mixing tend to reduce the number of unlike atomic pairs to lower the system energy. They therefore have apparently chemical spinodal decomposition in the liquid-amorphous state, leading to nanometre-scale clustering and compositional modulations. Interestingly, at

[1] Author to whom any correspondence should be addressed.

high strain rates, a positive-heat-of-mixing binary system with little solid solubility at about ambient temperature can become miscible at a lower temperatures [9].

The thermal behaviour of Pb inclusions in an Al matrix has been investigated over the past few decades [12–17]. Al–Pb alloy is an immiscible system even in the liquid state up to the monotectic temperature and has no intermediate phases in its phase diagram [23]. So it is a good model alloy for the study of physical properties of immiscible alloys. As early as 1969, Thackery and Nelson [10] first measured the particle shapes after ion-implantation and subsequent cooling from their liquid state at 400 °C. The particles were a few hundred nanometres in diameter and contained both {111} and {100} facets. Subsequently Mclean [11] studied the kinetics of spheroidization of long cylinders or rods of liquid Pb several micrometres in diameter by x-ray radiography. He found that spherical liquid inclusions larger than about 120 nm in diameter migrated in a temperature gradient, while smaller particles were immobile. The equilibrated particles tended to be spherical without apparent facets even during thermal migration. Moore *et al* [12, 13] investigated *in situ* liquid Pb inclusions in an Al matrix during heating by use of a transmission electron microscope (TEM) and found a significant increase of anisotropy at lower temperatures. Gabrisch *et al* [14] observed the shape of liquid Pb inclusions in an Al matrix over a wide range of sizes and temperatures by an *in situ* TEM investigation. They pointed out that the barrier of ledge nucleation necessary to advance the faceted interfaces could explain the observed dependence of particle shape on size and temperature.

Solid Pb inclusions in an Al matrix were found to adopt a cube–cube orientation relationship and formed defect-free precipitates in the shape of a cuboctahedron with eight {111} facets truncated by six {100} facets [12]. Recent studies [15–17] showed that the equilibrium shapes of solid Pb inclusions embedded in an Al matrix were also size dependent.

High resolution transmission electron microscopy (HRTEM) investigations of immiscible Pb–Al alloy samples prepared by a melt-spun method were carried out and interpreted in terms of crystallography by Zhang and Sui [18]. They found that, apart from some Pb inclusions with a cube–cube orientation relationship within an Al matrix in the shape of a cuboctahedron with eight {111} facets truncated by six {100} facets, the 'disorder' Al zones (around such Pb inclusions, strictly speaking, where the crystal order structure of Al matrix was disturbed). In general, they were larger than 20 nm in radius and existed in the samples aged for about two months.

2. Sample preparation and experimental results

An alloy ingot with a composition of Al–10 wt% Pb was prepared by arc melting of 99.999% pure Pb and Al in water-cooled copper crucibles under an Ar atmosphere. Rapidly solidified thin Pb–Al ribbons 2–3 mm wide, 40 μm thick and a few metres long were obtained by using a single roller melt spinning apparatus with a wheel speed of 25 m s^{-1} under Ar atmosphere. Some of the ribbons were aged at room temperature in order to observe micro-structural changes. The specimens were dimpled on a Gatan 565 dimpler and thinned by using Ar ion beam milling.

Figure 1 gives a typical HRTEM image of a Pb inclusion embedded in an Al matrix before ageing. The moiré patterns in figure 1 are caused by the difference in lattice parameters between the Pb inclusion and the Al matrix when they keep the cube–cube orientation relationship.

Interestingly, it was only after the samples had been aged for about two months that the disorder Al zones surrounding some Pb inclusions were found in the Al matrix. Figure 2(a) is a typical HRTEM image of such a microstructure. The thicknesses of these disorder Al zones are in the range 2–8 nm, which can be obtained by measuring a series of HRTEM images. This cube–cube orientation relationship between such Pb inclusions and the Al matrix still

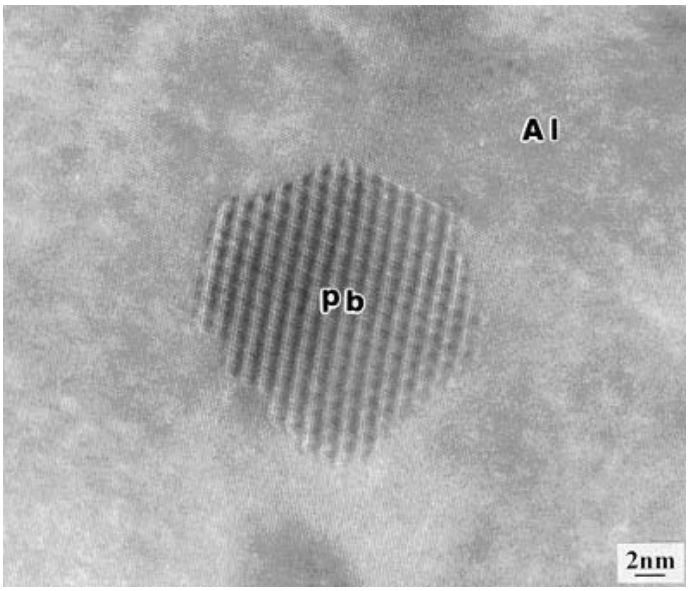

Figure 1. A typical HRTEM image of a Pb inclusion embedded in an Al matrix in the sample before ageing.

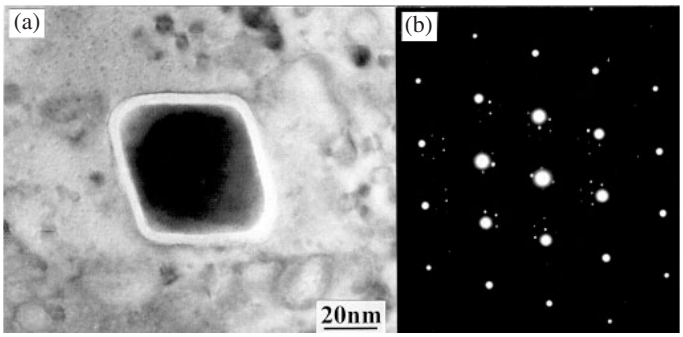

Figure 2. (a) A bright-field HRTEM image and (b) the corresponding selected area diffraction pattern (SADP) of the aged sample. A disorder Al zone around a Pb inclusion can be seen.

remains, and is further confirmed by the selected area electron diffraction (SAED) patterns shown in figure 2(b). In this figure, the stronger diffraction spot comes from the Al matrix and the weaker one comes from the Pb inclusion. An energy filtered image analysis (figure 3) finds evidence for the existence of a small amount of oxygen in the disorder zone. It is unclear why these disorder Al zones form, and it is difficult to clear them using only experimental methods. Therefore, it is necessary to explore them from the viewpoint of theoretical computation. In what follows, we will address the interpretation of the formation of disorder Al zones in an immiscible Pb–Al alloy by using the molecular dynamics (MD) method.

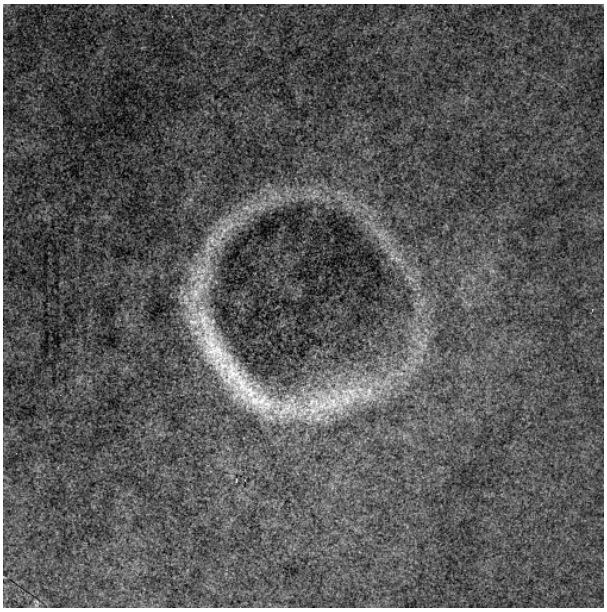

Figure 3. An energy filtered image of the sample with a disorder Al zone. The distribution of oxygen elements shows that a certain amount of oxygen exists in the disorder Al zone.

3. Interatomic potentials

In the following MD simulations, the Sutton–Chen (SC) many-body interatomic potentials [19, 20] are employed for the Pb–Al system. In the Sutton–Chen 'glue' scheme, the total energy E_{tot} for pure metals is expressed as a summation over atomic positions:

$$\begin{aligned} E_{\mathrm{tot}} &= \varepsilon\left[\tfrac{1}{2}\sum_{i\neq j} V(r_{ij}) - c\sum_i \rho_i^{1/2}\right], \\ V(r_{ij}) &= \left(\frac{a}{r}\right)^n, \\ \rho_i &= \sum_{j\neq i}\left(\frac{a}{r_{ij}}\right)^m. \end{aligned} \tag{1}$$

Here r_{ij} is the separation between atoms i and j, c is a positive dimensionless parameter, ε is a parameter with the dimensions of energy, a is a parameter with the dimensions of length, and m and n are positive integers. The pair potential V, is purely repulsive and the N-body term is purely cohesive. ρ_i is the local electron density around atom i.

The generalization of equation (1) to describe binary A–B alloys is straightforward by assuming that the interactions between like pairs are the same as in pure metals. The energy contributions of E_i^{AB} and E_i^{BA} to the ith atom (A or B) from unlike atoms (B or A) can be given as [21]:

$$\begin{aligned} E_i^{\mathrm{AB}} &= \tfrac{1}{2}\varepsilon^{\mathrm{AB}}\sum_{i\neq j} V^{\mathrm{AB}}(r_{ij}) - \varepsilon^{\mathrm{AA}}c^{\mathrm{AA}}(\rho_i)^{1/2}, \\ E_i^{\mathrm{BA}} &= \tfrac{1}{2}\varepsilon^{\mathrm{BA}}\sum_{i\neq j} V^{\mathrm{BA}}(r_{ij}) - \varepsilon^{\mathrm{BB}}c^{\mathrm{BB}}(\rho_i)^{1/2}. \end{aligned} \tag{2}$$

The parameters for this kind of potential are listed in table 1.

Table 1. Parameters for the Sutton–Chen potentials used for the Al–Pb system from [18–20].

	a (Å)	ε (eV)	c	m	n	δ
Pb–Pb	4.95	5.5765	45.7811	7	10	
Al–Al	4.05	9.1435	52.2066	5	9	
Pb–Al	4.48	7.1406		6	10	0.5

Table 2. Optimized EAM parameters for aluminium and oxygen from [21].

	A (eV)	ξ	r^* (Å)	α (Å)	β (Å)	B (eV)	C (eV)
Al–Al	0.763 905	0.147 690	3.365 875	1.767 488	2.017 519	0.075 016	0.159 472
O–O	2.116 850	1.000 000	2.005 092	8.389 842	6.871 329	1.693 145	1.865 072
Al–O			2.358 570	4.233 670	4.507 976	0.154 548	0.094 594

The embedded-atom method (EAM) approach [22] is chosen for the Al–O system. An EAM potential energy E_{tot} with the standard form

$$\begin{aligned} E_{\mathrm{tot}} &= \sum_i F_i(\rho_i) + \sum_{i<j} \phi_{ij}(r_{ij}), \\ F_i(\rho_i) &= -A_i\sqrt{\rho_i/\xi_i}, \\ \rho_i(r) &= \sum_{j\neq i} \xi_j \exp[-\beta_j(r_{ij} - r_j^*)], \\ \phi_{ij}(r) &= 2B_{ij}\exp\left[-\frac{\beta_{ij}}{2}(r - r_{ij}^*)\right] - C_{ij}[1 + \alpha(r - r_{ij}^*)]\exp[-\alpha(r - r_{ij}^*)], \end{aligned} \tag{3}$$

where $F_i(\rho_i)$ is the energy required to embed atom i in a local electron density ρ_i and $\phi_{ij}(r_{ij})$ the residual pair–pair interaction between i and j atoms separated by the interatomic distance r_{ij}. The corresponding parameters in equation (3) are summarized in table 2. In the calculation the interaction of Pb and O atoms is neglected because, for the aged samples, very low solubility of oxygen in the Pb inclusion could be found by the energy filtered image analysis.

4. Results and discussion

In this MD simulation of the formation of disorder Al zones, we will concentrate on explaining why disorder Al zones only exist around larger Pb inclusions in the aged samples and how they form. Before proceeding with the MD simulation for this problem, we should emphasize the following experimental facts, which will allow us to simplify the MD modelling and simulating without much computational effort. Firstly, the concentration of oxygen soluted in Pb inclusions of any size must be higher than that in the Al matrix at higher temperaturea. This is to be expected if we look at the preparation process of the samples. Oxygen soluted in a melt sample in a flowing Ar atmosphere with 1000 ppm oxygen impurity will reside in Pb inclusions and the Al matrix in a sequential rapid-cooling solidification process. The residual amount of oxygen depends on the solubility of oxygen in liquid Pb and Al phases. The fact that the solubility of oxygen in Pb (0.85% at 872 K) is much higher than that in Al (only about 0.1 at.% at 2054 K) [23], verifies the above expectation. During ageing at room temperature, the super-saturated oxygen would escape from Pb inclusions by diffusing into the Al matrix surrounding it. Secondly, the local stress gradients from a Pb inclusion to the Al matrix surrounding it would be produced due to the significant difference in shrinkage of volume between solid aluminium and lead in rapid solidification, which is caused by the difference in their expansion coefficients as listed in table 3. Thirdly, the cube–cube orientation relationship

Table 3. Thermal expansion coefficient and melting point for Pb and Al.

	Thermal expansion coefficient (ppm K^{-1})	Melting point (K)
Pb	29.10	600.60
Al	23.03	933.25

between some of the Pb inclusions and the Al matrix implies that one of the possible Pb/Al interfaces might be a semi-coherent one because both Pb and Al are face-centred cubic lattices with a 22% difference in lattice parameter (0.405 nm for Al and 0.495 nm for Pb).

The setup of the simulations of the formation of the disorder Al zone is as follows. A MD cell with x, y and z axes along three $\langle 100 \rangle$ crystallographic directions of lead is composed of an Al block, a Pb block and an interface between them as schematically shown in figure 4(a). We construct two kinds of possible initial interface on the x–y plane. As an example, a semi-coherent Pb/Al interface is shown in figure 4(b), which consists of 30 layers of Pb atoms with 162 atoms/layer and 38 layers of Al atoms with 242 atoms/layer. An orientation relationship of $Pb_{\{100\}} \parallel Al_{\{100\}}$ and $Pb_{\langle 100\rangle} \parallel Al_{\langle 100\rangle}$ between Al and Pb atomic layers is assumed. Based on the third experimental fact mentioned before, this assumption on the interface, for at least one of possible semi-coherent interfaces, might be reasonable. For presenting the effect of the interface configuration on the formation of the disorder Al zone, a kind of possible incoherent Pb/Al interface is also constructed, which consists of 30 layers of Pb atoms with 288 atoms/layer and 38 layers of Al atoms with 441 atoms/layer and has the orientation relationship of $Pb_{(001)} \parallel Al_{(001)}$, $Pb_{[100]} \parallel Al_{[110]}$ and $Pb_{[010]} \parallel Al_{[1\bar{1}0]}$. A periodic boundary condition is applied in the direction parallel to the Pb/Al interface and a soft boundary condition is applied in the direction perpendicular to the Pb/Al interface for the above two interfaces as shown in figure 4(a).

MD simulations are performed at a given temperature by using the Nose–Hoover method to control the system temperature [24]. The initial velocities of atoms in a MD cell are assumed to be in the Boltzmann distribution at the desired temperature. We choose a cutoff distance to be $2.5a_0$, namely, 2.5 times the lattice parameter of aluminium at 273 K, for all the simulations. In this method, the trajectory of each atom in a MD cell is followed through time and Newton's classical equations of motion with a time step $\Delta t = 1.0 \times 10^{-15}$ s are integrated in a step-wise manner over finite time steps in terms of a fifth-order, Nordsiek, predictor–corrector method [25]. The forces driving the motion of the atoms are computed from the gradient of the potential energy of the system with respect to the positions of each atom. The initial MD model with either the semi-coherent interface or the incoherent interface is relaxed to 50 000 steps in order to obtain an equilibrium configuration at a desired temperature.

The results of MD simulation without oxygen under any stress state demonstrate that there exists no disorder Al zones, which means that the existence of oxygen is responsible for the formation of such a disorder zone. In order to investigate where oxygen in the disorder Al zone comes from and how, we simulate the diffusing process of oxygen from the Pb block (like the Pb inclusion) to the Al block (like the Al matrix) through the semi-coherent or incoherent interface; we put a small amount of oxygen (about 12 oxygen atoms) in the interstitial sites between two Pb atomic layers near the interface in the equilibrium configuration relaxed previously. The simulation of diffusion of oxygen in the Al block along z axis direction is performed at 400 K. The simulation results shown in table 4 indicate that at 100 fs the diffusivity (D_s) of oxygen through the semi-coherent interface is much larger than the diffusivity (D_i) of oxygen through the incoherent interface. D_i drops sharply to about zero at 1 ps while at that time D_s remains at 10.0–13.0 $\times 10^{-5}$ cm^2 s^{-1}. D_s is no less than 0.05 $\times 10^{-5}$ cm^2 s^{-1} until 50 ps. To find

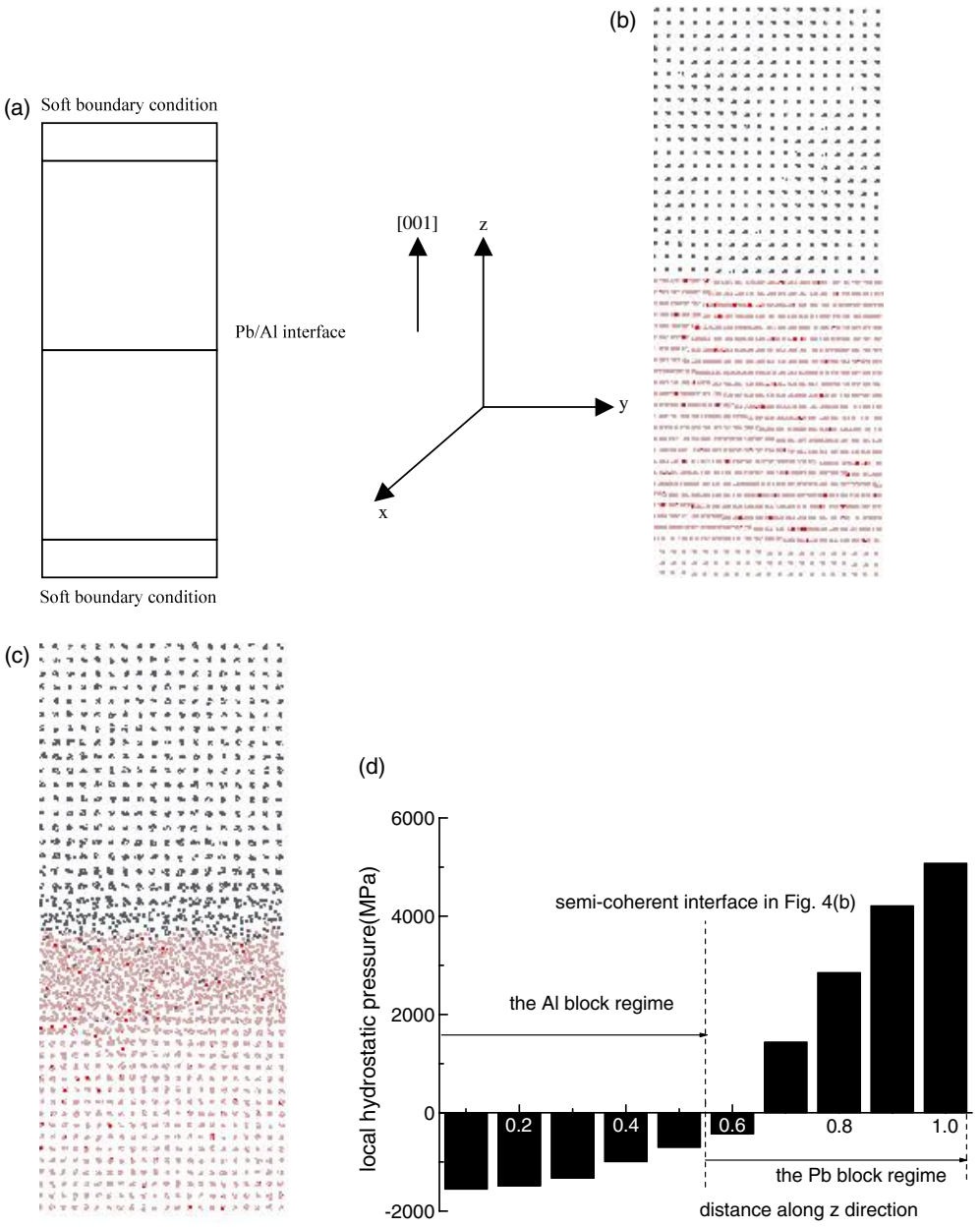

Figure 4. (a) Schematic diagram of the configuration of a MD cell used in MD simulation. A periodic boundary condition is applied in the direction parallel to the x–y plane and a soft boundary condition is applied in the direction perpendicular to the Pb/Al interface. (b) Initial unrelaxed configuration of a MD cell with a Pb/Al semi-coherent interface in which oxygen atoms are randomly distributed in twelve Al atomic layers near the interface by substituting some sites of aluminium atoms. (c) Equilibrium configuration after being relaxed to 80 000 steps. It is evident that a disorder Al zone appears in the Al matrix close to the semi-coherent interface. (d) Stress distribution along the z axis from the Pb block to the Al block in (c), where the stress value is the average one in a sublayer 1.512 nm wide and parallel to the x–y plane. It is seen that the Pb block is in a compressive stress state while the Al block is in a tensile stress state.

(This figure is in colour only in the electronic version)

Table 4. Diffusivity of oxygen in the Al matrix along the z axis direction with a semi-coherent interface (D_s) and an incoherent interface (D_i) in 10^{-5} cm^2 s^{-1}. D_{s1} is the diffusivity of oxygen under a compression stress state (801.0 MPa) while D_{s2} is the diffusivity of oxygen under a tensile stress state (−279.75 MPa).

	100 fs	1 ps	10 ps	50 ps
D_{s1}	12.57	10.44	0.36	0.15
D_{s2}	16.74	12.18	0.48	0.15
D_i	1.68	∼0.0	∼0.0	∼0.0

the influence of the stress state of the sample on the oxygen diffusion process (and on the formation of disorder Al zones) we calculate the diffusivities ($D_{s2} = 16.74 \times 10^{-5}$ cm s^{-1}) of oxygen through the semi-coherent interface in a tensile stress state (−279.75 MPa) and that ($D_{s1} = 12.57 \times 10^{-5}$ cm s^{-1}) in a compression stress state (801.0 MPa). D_{s2} is larger than D_{s1}, which means that oxygen more easily diffuses in a tensile stress state than in a compression stress state.

These computational results, even though obtained by means of the ideal and simple interface models, are not difficult to understand: the disorder of the arrangement of Pb and Al atoms in the incoherent interface will increase the diffusing resistance of oxygen atoms passing through such an interface. We may expect that this phenomenon would be more serious for a practical incoherent interface containing a large amount of defects, such as dislocations and vacancies. On the one hand, the trapped probability of oxygen atoms by such an incoherent interface is much larger than that by a semi-coherent interface in terms of the above comparison of the oxygen diffusivity through the two interfaces. On the other hand, the residence of a certain amount of oxygen in an incoherent Pb/Al interface is beneficial to the decrease of its higher interface energy (in general, about 800–2500 mJ m^{-2}, but it is about 200–800 mJ m^{-2} for a semi-coherent interface [26]).

From the above analysis, it is reasonable to conclude that the existence of oxygen in disorder Al zones for the samples with a semi-coherent interface between Pb inclusion and Al matrix, might be caused by the diffusion of oxygen from the Pb inclusion into the Al matrix due to a large D_s for oxygen passing through such an interface, especially in a tensile stress state. Moreover, with the fact that D_s in table 4 decreases with time in mind, we expect that oxygen atoms diffusing from the Pb inclusion would be distributed in a few or more than ten Al atomic layers, depending on the amount of oxygen soluted in the Pb inclusion at higher temperatures, or the size of the Pb inclusion.

In order to answer the question of whether it is possible to form such a disorder Al zone in the case of the existence of oxygen, in the following, for the sake of saving computational time, we will directly apply the above conclusions that oxygen exists in more than ten Al atomic layers near a semi-coherent interface to construct an initial MD cell with oxygen and then to simulate its variation.

Figure 4(b) shows, as an example, the initial MD cell in which 1.58 at.% oxygen is randomly distributed in 24 Al atomic layers close to the semi-coherent interface. Figure 4(c) gives the equilibrium configuration of this initial MD cell after being relaxed to 80 000 steps at 400 K, from which a disorder Al zone of about seven Al atomic layers wide can be seen. The final average tensile stress is 0.12 eV nm^{-3} and the stress distribution from the Pb block to the Al block along the z axis through the whole equilibrium configuration is plotted in figure 4(d). From this figure we see clearly that the Pb block is in a compression stress state while the Al block is in a tensile stress state. A stress gradient across the Pb/Al semi-coherent interface really exists, thus being in a good agreement with the deduction inferred from the second experimental fact. In order to clear the dependence of the thickness of the disorder

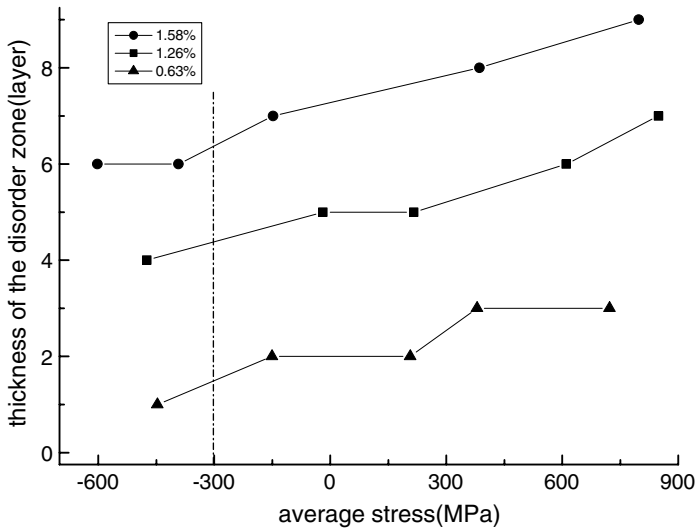

Figure 5. Plot of the thickness of the disorder Al zone versus the average stress in the equilibrium configuration of a MD cell. It increases nonlinearly with the gradual variation from a tensile (negative) stress state to a compression (positive) stress state.

Al zone on the average stress in the equilibrium configuration at a given amount (0.63, 1.26 and 1.58 at.% respectively) of oxygen, we perform a series of simulations by assuming the oxygen atoms dissolved in the Pb block to diffuse entirely into 24 atomic layers of Al close to the semi-coherent interface. The simulation results as plotted in figure 5 present the thickness of the disorder Al zone as a function of the average stress in the equilibrium configuration of a MD cell where the selected stress values correspond roughly to those caused by significant difference of Al and Pb volume shrinkage. At a certain amount of oxygen, the thickness of the disorder Al zone increases nonlinearly with average stress. Tensile stress (presenting a negative value in figure 5) might be beneficial to the extension of the disorder Al zone. The dash–dot line in figure 5 indicates that a small amount of oxygen would result in the formation of the disorder Al zone and the thickness of the disorder Al zone might be sensitive to the variation of the amount of oxygen.

Combining figure 5 with our simulation results that a disorder Al zone fails to form in an equilibrium configuration without oxygen in any stress state, we could conclude that the existence of oxygen in Al atomic layers close to the semi-coherent interface might be dominant enough to trigger the formation of a disorder Al zone. We also performed MD simulation without oxygen and found that a disorder Al zone failed to form in the equilibrium configuration without oxygen and stress.

In the process of melt spinning, only such Pb drops on the surface of the liquid alloy can solute oxygen from an Ar atmosphere. Because the time that Pb stays on the surface is different in spinning, the amount of oxygen in every Pb inclusion after rapid solidification will be different. This would be the reason why disorder Al zones exist for some Pb inclusions but not others.

5. Summary

In summary, on the basis of the above simulation results, we can imagine the sequence of events that would lead to the formation of the disorder Al zones observed experimentally.

The residual super-saturated oxygen soluted in Pb inclusions at higher temperatures readily diffuses into the Al matrix through a semi-coherent Pb/Al interface during ageing, but it is much more difficult through an incoherent interface. It is distributed in a few or more Al atomic layers close to this interface, depending on the amount of oxygen or the size of the Pb inclusion. The Al atomic layers containing a certain amount of oxygen would become an energetically favoured disorder Al zone in the equilibrium configuration. The stress gradient could be considered to strengthen the effect of oxygen on the formation of the disorder Al zone, which is secondary. Therefore only the existence of stress could not yield any disorder Al zone. Our computational results point out that the existence of oxygen in disorder Al zones, even though a small amount of oxygen, would be necessary for the formation of a disorder Al zone. The ultimate thickness of a disorder Al zone would be, therefore, mainly determined by the amount of oxygen soluted in the Pb inclusion at higher temperatures. The MD simulation results presented in this work provide a plausible explanation for the observed experimental phenomena.

Acknowledgments

This work was supported by the National Natural Science Fund of China (Grant No 50271071) and the Outstanding Young Research Fellowship (Grant No 50125103).

References

[1] Chattopadhyay K and Ramchandrarao P 1979 *Mater. Sci. Eng.* **38** 7
[2] Van Aken D C and Fraser H L 1985 *Acta Metall.* **33** 963
[3] Zhang D L and Cantor B 1990 *Phil. Mag.* A **62** 557
[4] Goswami R and Chattopadhyay K 1994 *Mater. Sci. Eng.* A **178–180** 163
[5] Nastasi M, Saris F W, Huang L S and Mayer J W 1985 *J. Appl. Phys.* **58** 3052
[6] Chen Y G and Liu B X 1996 *Appl. Phys. Lett.* **68** 3096
[7] Clemens B M and Hufnagel T C 1996 *Appl. Phys. Lett.* **69** 2938
[8] Kwon K W, Lee H-J and Sinclair R 1999 *Appl. Phys. Lett.* **69** 2938
Kwon K W, Lee H-J and Sinclair R 1999 *Acta Mater.* **47** 3965
[9] Sheng H W and Ma E 2001 *Phys. Rev.* B **63** 224205
[10] Thackery P A and Nelson R S 1969 *Phil. Mag.* **19** 169
[11] McLean M 1973 *Phil. Mag.* **27** 1253
McLean M *et al* 1974 *J. Mater. Sci.* **9** 1104
[12] Moore K I, Chattopadhyay K and Cantor B 1987 *Proc. R. Soc.* A **114** 499
[13] Moore K L, Zhang D L and Cantor B 1990 *Acta Metall. Mater.* **38** 1327
[14] Gabrisch H, Kjeldgagrd L, Johnson E and Dahmen U 2001 *Acta Mater.* **49** 4259
[15] Zhang D L and Cantor B 1990 *Scr. Metall.* **24** 751
[16] Anderson H H and Johnson E 1995 *Nucl. Instrum. Methods* B **106** 480
[17] Johnson E, Johansen A, Hinderberger S, Xiao S-Q and Dahmen U 1996 *Interface Sci.* **3** 279
[18] Zhang L H and Sui M L 2004 *Appl. Phys. Lett.* at press
[19] Sutton A P and Chen J 1990 *Phil. Mag. Lett.* **61** 139
[20] Raf II-Tabar H and Sutton A P 1991 *Phil. Mag. Lett.* **63** 217
[21] Jin Z H, Sheng H W and Lu K 1999 *Phys. Rev.* B **60** 141
[22] Streitz F H and Mintmire J W 1994 *Phys. Rev.* B **50** 11996
[23] *Binary Alloy Phase Diagrams* 1992 2nd edn (ASM, Ohio: Materials Information Society) p 2902
[24] Nose S 1984 *Mol. Phys.* **2** 255
[25] Adler B J and Wainwright T E 1959 *J. Chem. Phys.* **31** 459
[26] Howe J M 1997 *Interface of Materials* (New York: Wiley) p 378